Crystal Structure and Optical Properties of a Homometallic Heterotrinuclear Europium(III) Complex – a Cationic Eu(III) ion Coordinated by two $[Eu(III)DOTA]^-$ Complexes

Maria Storm Thomsen,[a] Anders Ø. Madsen,[b] & Thomas Just Sørensen [a]*

[a)] Nano-Science Center and Department of Chemistry, University of Copenhagen, Universitetsparken 5, 2100 København Ø, Denmark, tjs@chem.ku.dk

[b)] Department of Pharmacy, University of Copenhagen, Universitetsparken 2, 2100 København Ø, Denmark

KEYWORDS: Lanthanide luminescence, europium(III) ion, crystal structure, homometallic, heteronuclear.

The structure and solid state luminescence properties of a homometallic heterotrinuclear $[Eu(\mu O)_5(OH_2)_3][Eu(DOTA)(H_2O)]_2Cl$ crystal was determined and was found to have two sites: a free europium(III) ion and a $[Eu(DOTA)(H_2O)]^-$ complex. The trinuclear compound crystallizes in a laminar structure in triclinic space group $P\bar{1}$. The crystal structure was determined using complex data treatment due to non-merohedric twinning. Experimental data sets were recorded with

large redundancy and separated according to scattering domain in order to obtain a reliable structure, which revealed the configuration of the europium(III) sites. In first site, the europium(III) 1,4,7,10-tetrazacyclododecane-1,4,7,10-tetraacetate (Eu.DOTA) complex was found to adopt a capped twisted square antiprismatic (cTSAP) conformation, where a capping water molecule increased the coordination number of the europium(III) site to nine (CN = 9). In the second site, the cationic europium(III) ion was found to be coordinated by three water molecules and five oxy groups from neighboring $[Eu(DOTA)(H_2O)]^-$ complexes. The coordination geometry of this site was found to be a compressed square antiprism (SAP), and the coordination number of the europium(III) ion was found to be eight (CN = 8). A large increase in rate constant of luminescence was observed for Eu(III) in $[Eu(DOTA)(H_2O)]^-$ in solid state luminescence spectroscopy measurements compared to in solution, which lead to investigations of single-crystals in deuterated media to exclude additional effects of quenching. We conclude that the most probable cause of the decrease in observed luminescence lifetimes is the high asymmetry of the coordination environment of $[Eu(DOTA)(D_2O)]^-$ in the $[Eu(\mu O)_5(OD_2)_3][Eu(DOTA)(D_2O)]_2Cl$ crystals.

INTRODUCTION

Lanthanides are essential in modern technology and are indispensable in fields ranging from catalysis,[1-2] metallurgy,[3] to organic synthesis,[4] and bio-imaging.[5-6] Thus, there is a constant increase in the demand for almost all rare-earth elements, including the lanthanides.[7] To meet the demand, the lanthanides either have to be integrated in a closed circular economy,[8] or the solvo-hydrometallurgy used for rare-earth purification and separation must be optimized.[9] Both options require a deeper understanding of the structure-property of the lanthanide ions. In particular, knowledge of the solution chemistry of the trivalent lanthanide ions.

The fast ligand-exchange kinetics complicates the study of lanthanide(III) solution chemistry.[10-17] In the solid state, there is a strong understanding of structure-property relationships,[18] but the increased degree of freedom in solution often results in an averaging of the observed properties. This makes structure determination difficult,[15, 19-20] and complicates attempts of linking a specific property to a give structure.[16, 21] To resolve this issue, we can crystallize a lanthanide complex in the structure we perceive as the average structure in solution,[22-24] and use solid state spectroscopy on

these 'locked' model systems to provide information on the properties of specific geometries. Thus, allowing us to correlate the known structures in crystals with properties observed in solution.

In this paper, we present a crystal structure of the homometallic heterotrinuclear europium(III) complex $[Eu(\mu O)_5(OH_2)_3][Eu(DOTA)(H_2O)]_2Cl$ (**1-H,** DOTA = 1,4,7,10-tetraazacyclododecane-1,4,7,10-tetraacetate),[25] which contains different two europium(III) sites. The general structure of these two sites is illustrated in Figure 1.

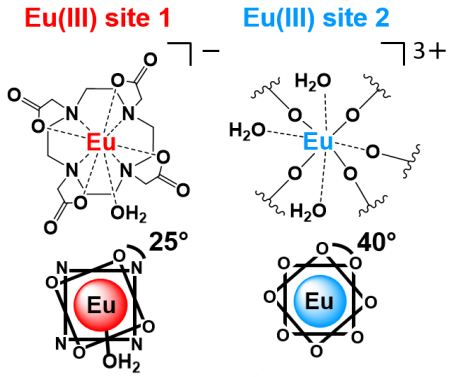

Figure 1. The two Eu(III) sites in **1-H**. Eu(III) site 2 is coordinated by carboxylate arms in five neighboring Eu.DOTA complexes as illustrated by wiggly lines.

Due to a strong red luminescence, europium(III) has been extensively used to study the *f-f* transitions of lanthanide(III) ions,[18, 26-31] and as a consequence numerous crystal structures or europium(III) complexes with different counter-ions, coordination numbers, coordination geometries and donor atoms have been reported.[31-37]

The DOTA ligand is the safest scaffold to use in diagnostic gadolinium(III) enhanced MRI,[5, 13, 38-40] and the solution structure of $[Ln(DOTA)]^-$ has been studied in great detail. The structure of **1-H** was discovered as part of a project aimed at crystallizing $[Ln(DOTA)]^-$ in the twisted square antiprism (TSAP) geometry in order to resolve the distinct optical properties of the two structures $[Ln(DOTA)]^-$ predominately adopts in solution: a capped square antiprism (cSAP), and a capped twisted square antiprism (cTSAP).[15, 25, 41-43] The two nine-coordinated complexes differ in the twist angle between the N- and O-donor planes. In the SAP form the twist angle is ~40º, while it is between 25-30º in TSAP form.[22, 44] The consequence of this minor change in coordination geometry has proven difficult to study without comparing different ligand systems. But as the lanthanide(III) ions are largely indifferent towards the directionality of ligand donation, it crystal packing can enforce different coordination environments. Here, we exploit this to study the changes in the optical properties of europium(III) induced by variations in the coordination geometry of $[Eu(DOTA)(D_2O)]^-$ complexes. Further, to the best of our knowledge, this is the first report of a crystal structure of a europium(III) DOTA complex in the cTSAP form. Similarly, we believe that this is the first example of a homometallic heterotrinuclear europium(III) complex, where the europium(III) complexes act as both cation and anion.

EXPERIMENTAL METHODS

Materials. All chemicals were used as received. For Eu(III) sources: 99.9% $EuCl_3 \cdot 6H_2O$ from abcr, 98% $Eu(CF_3SO_3)_3$ from STREM Chemicals.

Synthesis of 1-H. $Na[Eu(DOTA)H_2O]$ was made according to the protocol developed by Desreux. To crystallize **1-H**, a solution was prepared by dissolving 100 mg of $Na[Eu(DOTA)H_2O]$ in 3 mL water. The pH was lowered to 4-5 by addition of 1 M HCl

(from diluting concentrated HCl 37% with deionized water) and controlled using pH indicator paper (Macherey Nagel), prior to the addition of 150-300 mg of an Eu(III) source ($EuCl_3 \cdot 6H_2O$, $Eu(CF_3SO_3)_3$ were used). The amount of added Eu(III) salts was adjusted according to the perceived amount of water in the salt, that is, a smaller amount of dry salts was used, while the high end of the interval was used for hydrates. The pH of the final solution was then adjusted to ~3 by addition of 1 M HCl and 2 M NaOH to a final volume of 4.5 mL. The pH was controlled using a pH meter (Mettler Toledo InLab Expert Pro ISM), and the solution was taken up in a syringe, and filtered (Frisenette QMax RR syringe filters 13 mm PTFE hydrophilic) into a 10 mL vial (24 mmØ x 41 mm). The aqueous solution was placed in a 70 mmØ crystallization dish containing 50 mL of acetone. The diffusion chamber was covered by a 115 mmØ crystallization dish and left for acetone diffusion until the total volume in the vial was ~6 mL. When left at room temperature thin, fragile, plates of flaked white crystals appears in the vial over a few days. The thin plates are arranged in a layer structure, which complicated structure determination by single-crystal X-ray diffraction.

Synthesis of 1-D. 100 mg of $Na[Eu(DOTA)H_2O]$ and 150 mg of $Eu(CF_3SO_3)_3$ was dissolved in DCl (37%, Sigma-Aldrich) diluted with deuterium oxide (Euriostop) with a resulting pH = 1. The pH was adjusted with diluted solutions of DCl and NaOD (diluted from 37% DCl and 40 wt.% NaOD, Sigma-Aldrich) until pH was ~3. The solution of 6 ml was taken up into a syringe, and filtered (Frisenette QMax RR syringe filters 13 mm PTFE hydrophilic) into a 20 mL vial (27 mmØ x 55 mm). The aqueous solution was placed in a 70 mmØ crystallization dish containing 50 mL of acetone. The diffusion chamber was covered by a 115 mmØ crystallization dish and left for acetone diffusion until the total volume in the vial was ~9 mL. Flaked white crystals appear in the vial over a few days.

Single crystal X-ray diffraction and structure determination. Single crystal X-ray diffraction data were collected on a Bruker D8 VENTURE diffractometer equipped with Mo Kα high brilliance IμS radiation X-ray tube (λ = 0.71073 Å), a multilayer X-ray mirror, a PHOTON 100 CMOS detector, and an Oxford Cryo Systems low temperature device. The diffractometer was controlled using the SAINT program as implemented in the APEX2 software package.[45] Due to assumed non-merohedric twinning, the unit cell dimensions and orientation matrices were determined with *CELL_NOW*,[46] while absorption correction and generation of detwinned and summed intensity data files was done with *TWINABS*.[47] The structure was solved using Olex2[48] with the ShelXS solution program[49] using direct methods and refined with the ShelXL refinement package[50] using least-squares minimization. Non-hydrogen atoms were refined anisotropically, whereas hydrogen atoms were placed at calculated positions and were refined using a riding model.

Powder X-ray diffraction. Powder X-ray diffraction was performed on a dried sample from isolated crystals that were crushed between two microscope slides and measured on a low background silica sample holder. Data was collected on a Bruker D8 Advance diffractometer fitted with suitable optics and a Cu X-ray tube.

Optical spectroscopy and luminescence lifetime determination. Steady-state measurements were performed on both single crystals and powdered samples using a PTI QuantaMaster8075 from Horiba Scientific with a xenon arc lamp as excitation source. Excitation spectra were recorded with emission detected at 614 nm with excitation and emission slits at 1.5 and 8 nm, respectively. Emission spectra were recorded with excitation at 394 nm with excitation and emission slits at 8 and 1.5 nm respectively. Measurements on single crystals were done at room temperature. Dried powder samples were measured in a 2:5 propanol:diethyl ether glass in a NMR tube in a cold-finger setup containing liquid nitrogen. A constant nitrogen flow in the sample chamber was used to avoid ice formation.

Time-resolved luminescence measurements were performed on the same system, but with a xenon flash lamp as the excitation source. The point of excitation was 394 nm, and the emission was detected at 614 nm. Excitation and emission slits were both set at 8 nm. Lifetime traces were fitted to either a mono- or a bi-exponential decay model using the Origin 2017 software package.[51]

RESULTS

Non-merohedric twinning and structure determination. Twinning is often inaccurately used to describe fragmented crystals based on their split reflection profiles alone.

Table 1. Selected crystallographic data – 1-H.

Domain 1 – Solution and refinement HKLF 4 file			
Empirical formula	$C_{32}H_{73}ClEu_3N_8NaO_{32.1}$	ρ_{calc}g/cm^3	1.984
Formula weight	1597.90	μ/mm^{-1}	3.634
Temperature/K	100	F(000)	1590.0
Crystal system	Triclinic	Crystal size/mm^3	1.198 × 0.711 × 0.12
Space group	$P\bar{1}$	Radiation	MoKα (λ = 0.71073)
a/Å	9.2252(18)	2Θ range for data collection/°	3.196 to 51.358
b/Å	16.937(3)	Reflections collected	9966
c/Å	17.274(4)	Independent reflections	9966 [R_{int} = Merged, R_{sigma} = 0.0407]
α/°	96.37(3)	Data/restraints/parameters	9966/866/716
β/°	92.39(3)	Goodness-of-fit on F^2	1.037
γ/°	93.26(3)	Final R indexes [I>=2σ (I)]	R_1 = 0.0625, wR_2 = 0.1589
Volume/Å^3	2674.9(9)	Final R indexes [all data]	R_1 = 0.0814, wR_2 = 0.1720
Z	2	Largest diff. peak/hole / e Å^{-3}	3.92/-1.97

Twinned crystals must be individual aggregates, but be joint in a mutual orientation.[52] For non-merohedric twins the reciprocal lattices do not necessarily overlap, which often makes it possible to observe twinning during the initial data collection. This was the case for all isolated crystals of **1-H**, however, it was not possible to isolate a non-twinned crystal for structure determination. The nature of the initial reflections along with failed auto-indexing and an unusually long unit cell axis suggested possible non-merohedric twinning, and the subsequent collection of data was treated as such.[53] Out of several, the crystal with the most unanimous auto-indexing of the unit cell was chosen. A data set with a large redundancy of reflections was collected to ensure a high completeness after domain separation. *CELL_NOW* was used to identify the best fitting unit cell and the reflections that fit the cell was assigned to domain 1. The initial unit cell was then rotated to locate twin domains in the remaining reflections. By this approach, both the orientation matrices and twin laws were found simultaneously. Three domains were found, and the orientation matrices of the first two are related by 180º. Following integration of the reflections, multi-scan absorption correction by *TWINABS* was performed on all three domains. Both detwinned HKLF 4 and twinned HKLF 5 data files were generated, however, detwinning before refinement (against the HKLF 4 data) appeared more robust, and the data quality indicators were better than for the HKLF 5 data prepared for twin refinement. The precise reason for this is unknown, however, the problem presumably occurs during the summing of intensities for the generation of the HKLF 5 file. Since refinement against HKLF 5 works best if all domains are of similar quality, the HKLF 4 file was used for both the structure solution and refinement.[53] Structure information is given in Table 1.

Crystal structure and packing. The complex $[Eu(\mu O)_5(OH_2)_3][Eu(DOTA)(H_2O)]_2Cl$ **(1-H)** crystallizes in the triclinic space group $P\bar{1}$ with the unit cell dimensions a = 9.2252(18), b = 16.937(3), c = 17.274(4) Å, α = 96.37(3), β = 92.39(3), γ = 93.26(3)º and V = 2674.9(9) Å^3. The deuterated system, **1-D,** was confirmed as isostructural with **1-H** by unit cell determination. The unit cell is comprised of two enantiomeric complexes, which are charge balanced by chloride. Additional solvent molecules and sodium ions are present in the structure (see Table 1). The asymmetric unit is a single homometallic heterotrinuclear complex as shown in Figure 2, which also shows the coordination geometry and the twist of the donor-atom planes in the two square antiprisms. The complex has three europium(III) atoms in two sites: the nine coordinated $[Eu(DOTA)(H_2O)]^-$ complexes are in site 1 (Eu.**S1**), and the eight coordinated $[Eu(\mu O)_5(OH_2)_3]^{3+}$ complexes are in site 2 (Eu.**S2**).

Eu.**S1** is nine-coordinated with eight donor atoms from the DOTA ligands and a capping water. The coordination geometry is a capped twisted square anti-prism (cTSAP), where the metal is coordinated by four nitrogen and five oxygen atoms (Figure 2). The twist angle between the N- and O-donor planes are 25.3º and 26º for the two $[Eu(DOTA)(H_2O)]^-$ complexes in the asymmetric unit. Both $[Eu(DOTA)(H_2O)]^-$ complexes have the same chirality Δ(δδδδ),[6] and are in the unit cell mirrored by the set of the other enantiomer in the second homometallic heterotrinuclear complex in the unit cell (see Supporting Infor-

mation Figure S3). There are minor differences in bond lengths (Table 2) between the two $[Eu(DOTA)(H_2O)]^-$ complexes, however, they are treated as optically equivalent and are collectively referred to as Eu.**S1**.

In Eu.**S2,** the europium(III) ion is eight coordinated and adopts a square anti-prism (SAP) coordination geometry (Figure 2). The Eu(III) ion is coordinated to eight oxygen atoms, of which three are water molecules and five are from carboxylate arms on five surrounding $[Eu(DOTA)(H_2O)]^-$ complexes. The square antiprismatic structure is significantly distorted from the ideal as the two square donor sets are leaning towards a rhomboid, where the twist angle between two O-donor planes is ~40º.

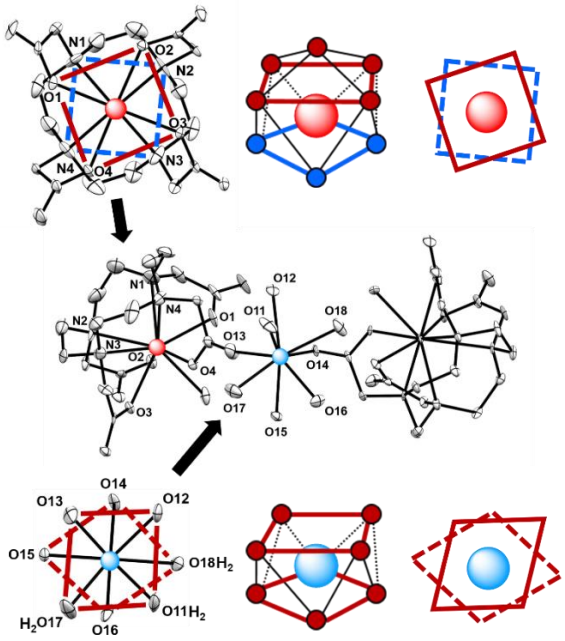

Figure 2. Crystal structure of the asymmetric unit in **1-H** showing the two different Eu(III) sites. **Top:** Eu.DOTA (**Eu.S1**) showing the N- and O-donor atom planes. Red = front oxygen plane, blue (dashed) = back nitrogen plane. **Bottom:** $Eu(\mu O)_5(OH_2)_3$ (**Eu.S2**) showing the O-donor atom planes. Red = front oxygen plane, red (dashed) = back oxygen plane.

The crystal packing in **1-H** is a layered structure, where each homometallic heterotrinuclear $[Eu(\mu O)_5(OH_2)_3][Eu(DOTA)(H_2O)]_2Cl$ complex spans the layer and form an interconnected sheet that only exposes the hydrophobic surface of the $[Eu(DOTA)(H_2O)]^-$ complexes to the interlayer interface. The interface is occupied by solvent molecules, and sodium and chloride ions. See Supporting Information for details.

Table 2. Eu-O and Eu-N bond lengths in 1-H crystal structure.

Eu(III) site	Atom1	Atom2	Distance (Å)
Site 1.1[a]	Eu1.1	N1	2.654(5)
Site 1.1	Eu1.1	N2	2.657(9)
Site 1.1	Eu1.1	N3	2.690(3)
Site 1.1	Eu1.1	N4	2.697(6)
Site 1.1	Eu1.1	O1	2.362(4)
Site 1.1	Eu1.1	O2	2.387(6)
Site 1.1	Eu1.1	O3	2.408(3)
Site 1.1	Eu1.1	O4	2.376(5)
Site 1.1	Eu1.1	O5[b]	2.530(5)
Site 1.2	Eu1.2	N5	2.702(2)
Site 1.2	Eu1.2	N6	2.639(3)
Site 1.2	Eu1.2	N7	2.646(2)
Site 1.2	Eu1.2	N8	2.637(7)
Site 1.2	Eu1.2	O6	2.365(8)
Site 1.2	Eu1.2	O7	2.387(6)
Site 1.2	Eu1.2	O8	2.374(6)
Site 1.2	Eu1.2	O9	2.399(8)
Site 1.2	Eu1.2	O10[b]	2.541(3)
Site 2	Eu2	O11[b]	2.417(0)
Site 2	Eu2	O12	2.469(4)
Site 2	Eu2	O13	2.303(6)
Site 2	Eu2	O14	2.332(9)
Site 2	Eu2	O15	2.426(1)
Site 2	Eu2	O16	2.410(5)
Site 2	Eu2	O17[b]	2.407(3)
Site 2	Eu2	O18[b]	2.496(9)

[a] Site 1.1 and 1.2 refers to the two Eu.DOTA centers in the asymmetric unit. [b] Water molecule.

Luminescence lifetimes. A crystal of **1-H** was isolated and the unit cell dimensions were determined with X-ray diffraction to confirm consistency with the dimensions found in the structure determination. The luminescence lifetime and optical properties were measured on the isolated single crystal (see Figure S2 for setup). As there are two Eu(III) sites in the structure (Eu.**S1** and Eu.**S2**), we expect to observe two luminescence lifetimes. A short lifetime is expected from Eu.**S2**, due to quenching from the water molecules. A longer luminescence lifetime is expected from Eu.**S1**. The argument can also be carried out using *q*, the number of inner sphere solvent molecules,[54-56] where *a priori* Eu.**S1** should have $q = 1$ and Eu.**S2** should have $q = 3$.

The luminescence lifetime was determined by recording the time-resolved emission decay profile from the single crystal and fitting the data to a biexponential decay model (All data available in the SI). The result is compiled in Table 3. The first lifetime is 88.3 μS, which is shorter than the 100 μS lifetime reported for $Eu(OH_2)_9^{3+}$ in water.[57-58] The second **1-H** single crystal lifetime was determined at 460 μS, which also is significantly shorter than the reported 663-667 μS for $[Eu(DOTA)(H_2O)]^-$ in water.[59-60]

A powder sample of **1-H** was prepared to ensure the single-crystal structure was representative of the bulk sample (see Figure S5 for powder X-ray diffractogram), and to eliminate the orientation effects observed in the single crystal experiment *vide infra*. Further, the powder sample allowed for the luminescence lifetime to be determined at 77K. The time-resolved emission decay profile recorded from the cold powder clearly showed two unique lifetimes (see Figure S7). The shorter lifetime was determined to be 267 μS, which is close to three times longer than in the single crystal at 293 K. The longer lifetime was determined to

be 558 μS, and thus remains significantly shorter than the lifetime determined for $[Eu(DOTA)(H_2O)]^-$ in water at 293 K.

Table 1. **Luminescence lifetimes of Eu(III) in a 1-H crystal, 1-H powder and a 1-D crystal at two different positions.**

	Temp. (K)	τ_1 (μS)	τ_2 (μS)
1-H	293	88.3	460.3
Powder 1-H	77	267.2	558.5
1-D @Position1	293	-	880.7
1-D @Position2	293	559.1	962.2

Amin *et al.* has studied the luminescence lifetimes of $[Eu(DOTAM)(H_2O)]^{3+}$ (DOTAM = l,4,7,10-tetraazacyclododecane-l,4,7,10-tetraacetamide).[61] The structure has a similar TSAP geometry around the Eu(III) center as **1-H**, with a twist angle between the N- and O-donor planes of 30.4º. The Eu-O_{water} bond length for Eu.DOTAM is 2.44 Å, which is shorter than in Eu.**S1** in **1-H**. They report a lifetime for $[Eu(DOTAM)(H_2O)]^{3+}$ of 518 μS in water, which is closer to the value for **1-H** than the lifetime reported for SAP $[Eu(DOTA)(H_2O)]^-$. The difference in lifetime has up to this point been ascribed to quenching from the amide N-H osccilators.[55]

Deuterated crystals (**1-D**) were made to increase luminescence intensity. An isolated single crystal was measured in the same setup as described for **1-H**. Noticeable orientation effects were observed when changing the position of the crystal surface towards the incident beam by rotating the platform supporting the single crystal. The crystal was rotated 360 degrees clockwise in increments of 10 degrees, and time-resolved emission decay profiles were recorded at every increment. Table 3 shows the lifetimes determined from these data at two specific orientations of the crystal. At one orientation (position 1) only one lifetime of 880 μS was observed. It is significantly lower than the lifetimes of both $[Eu(DOTA)(H_2O)]^-$ and $[Eu(DOTAM)(H_2O)]^{3+}$ determined in D_2O, that is 2,174 μS and 2,439 μS respectively.[59-61] Two lifetimes were determined at a second orientation (position 2). The longer lifetime of 962.2 μS remains shorter than both $[Eu(DOTA)(H_2O)]^-$ and $[Eu(DOTAM)(H_2O)]^{3+}$ in D_2O. The shorter lifetime was determined to be 559.1 μS, which is close to a fourth of the value reported for $Eu(D_2O)_9^{3+}$ of 2,270 μS.[58]

Luminescence spectra. The normalized emission spectra of all three are shown in Figure 3.

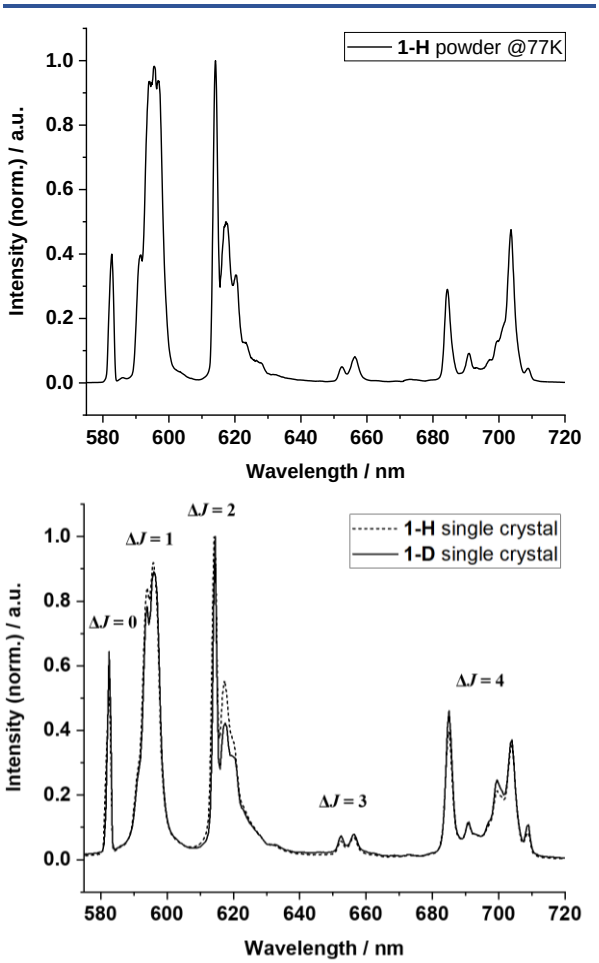

Figure 3. Top: Normalized steady-state emission spectra of **1-H** powder at 77K. **Bottom:** Normalized steady-state emission spectra of single crystals of **1-H** and **1-D** at a random orientation. (Excitation = 394 nm, slits = 8 nm)

Excitation and emission spectra were measured from a **1-H** crystal, a powder sample of **1-H**, and a **1-D** crystal. The powder sample was recorded at 77K, whereas the crystals were measured in the same setup as described for the time-resolved measurements at 293K. The spectrum of the powder is better resolved and shows that the $\Delta J = 1$ and $\Delta J = 2$ bands consist of several transitions. For the $\Delta J = 1$ band more transitions than the three that is possible in a single Eu(III) site is observed. In contrast, the spectra from the single crystals show fewer lines in the $\Delta J = 1$ and $\Delta J = 2$ bands. The loss of orientation effects in the powder compared to the crystal spectra is clearest in transitions of the $\Delta J = 4$ band, where there is a clear shift in the intensity in the 685 nm and 704 nm lines. These lines are highly sensitive to the orientation of the crystal *vide infra*.

Resolving spectra of the Eu.S1 and Eu.S2 sites. When recording the luminescence spectra from the single crystal of **1-H** at different orientations, we noted that the emission intensity of each line in the spectrum changed with the orientation of the crystal. Therefore, the effect of orientation was investigated using the deuterated complex, **1-D**. Emission spectra were recorded from the two orientations identified via the observation of distinct luminescence lifetimes (Table 3). The time-resolved emission decay profiles and the emission spectra determined at these two orientations are shown in Figure 4.

The spectrum at position 1 corresponds to the decay with only one lifetime, and the emission profile resembles those previously reported for $[Eu(DOTA)(H_2O)]^-$.[59, 62] Therefore, we conclude that the emission and lifetime at position 1 are strongly dominated by emission from Eu.**S1.** The second spectrum corresponds to the decay with two lifetimes. The features of $[Eu(DOTA)(H_2O)]^-$ transitions remain prominent, however, the ratio between the line intensities for the transitions observed in the $\Delta J = 4$ band are closer to those found in spectra of $Eu(H_2O)_9^{3+}$.[16] Thus, we conclude that the emission spectrum observed at position 2 is a composition of the spectra of both Eu.**S1** and Eu.**S2**.

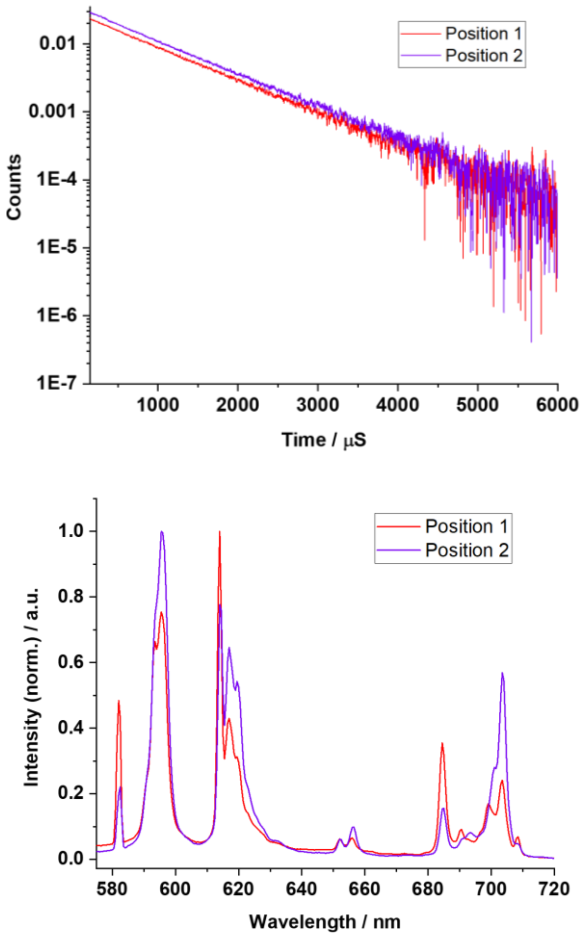

Figure 3. Top: Lifetimes of **1-D** at position 1 (red) and position 2 (purple). Excitation = 394 nm. Emission = 614 nm. **Bottom:** Normalized emission spectra of **1-D** at position 1 (red) and position 2 (purple). Excitation = 394 nm

DISCUSSION

The crystal structure. The bond lengths in $[Eu(DOTA)(H_2O)]^-$ Eu.**S1** for Eu-O and Eu-N in **1-H** are shown in Table 2. For both Eu-N in the cyclen ring and Eu-O from the carboxylate arms, the bond lengths are similar to what is found in structures of SAP $[Eu(DOTA)(H_2O)]^-$,[44, 63] and TSAP $[Eu.DOTMA]^{3+}$ (DOTMA =1*R*,4*R*,7*R*,10*R*- α,α′,α″,α‴- tetramethyl-1,4,7,10 tetraazacyclododecane-1,4,7,10-tetraacetate). [64] The Eu-O_{water} bond length is on average 2.535 Å, which is slightly longer than other reported values of 2.483 Å and 2.389 Å for SAP $[Eu(DOTA)(H_2O)]^-$ with sodium and uranyl oxalates as counter ions, respectively. [44, 63] It is, however, comparable to the Eu-O_{water} bond length of 2.558 Å in the TSAP DOTA-derivative $[Eu.DOTMA]^{3+}$.[64]

Four structures of TSAP $[Ln.DOTA]^-$ are reported in the Cambridge Crystallography Data Center database by Benetollo *et al.*, Aime *et al.*, and Thuéry.[44, 63, 65] The structures have Ln = La, Ce, Gd and Tm, where the Ce structure has a capping water molecule (cTSAP) and the other three does not (TSAP). The Ln-N and Ln-O bond lengths in $[La.DOTA]^-$ and $[Ce.DOTA]^-$ are longer than for **1-H,** which is easily rationalized by the larger ionic radius of La(III) and Ce(III) compared to Eu(III).[66] The Ce-O_{water} bond length of 2.59 Å is also longer than in **1-H**. The twist angle between the N-O-atom donor plane is 25.4º (Ce) and averaged at 22º (La). In Gd.DOTA and Tm.DOTA the Ln-N and Ln-O bond lengths are shorter than in **1-H**, which is agreement with the smaller ionic radii of Gd(III) and Tm(III) compared to Eu(III).[66] Here, the twist angle between the N-O-atom donor plane is 23.9º (Gd) and 24.5º (Tm).

The TSAP form of Ln.DOTA is rare in the solid state, but the few reported cases include both the larger and the smaller lanthanides. Generally, the size of the Ln(III) ion dictates the geometry in a series of lanthanide complexes with the same ligand system. Nevertheless, the cTSAP conformation of $[Eu(DOTA)(H_2O)]^-$ in **1-H** and the other TSAP Ln.DOTA structure indicates that crystal packing strongly influences which conformation the complex will adopt in the solid state.

Relating structure to property. All the lifetimes found for both **1-H, 1-H** powder and **1-D** (Table 3) are lower than reported values for $[Eu(DOTA)(H_2O)]^-$ in H_2O and D_2O.[58-60] This can be caused by two factors. Quenching by phonons in the crystal lattice or increased asymmetry around the Eu(III) centers, which causes mixing of states and makes the optical transitions more allowed, resulting in an increased rate constant of luminescence, k_{Lm}. [27] This leads to a higher luminescence intensity and lower luminescence lifetime as k_{Lm} increases:

$$\tau_{Lm} = (k_{Lm} + k_{nr})^{-1} \qquad \text{(eq. 1)}$$

$$\phi_{Lm} = k_{Lm}(k_{Lm} + k_{nr})^{-1} \qquad \text{(eq. 2)}$$

Where k_{nr} is the collective rates of non-radiative deactivation, τ_{Lm} is the luminescence lifetime, and ϕ_{Lm} is the luminescence quantum yield of europium(III) centered emission. The absorption spectrum of **1-H** (see Figure S9) shows no (optically active) phonons, so we conclude that the reduction of the luminescence of the europium(III) centers is not caused by lattice vibrations. Also, calculating the number of inner sphere solvent molecules for $[Eu(DOTA)(H_2O)]^-$ Eu.**S1** yields $q = 1$.[54-56] It is unlikely that high-energy phonons are not perturbed upon proton-to-deuterium exchange. Therefore, we see this as additional support for our hypothesis that the decreased luminescence lifetime observed in **1-H** and **1-D** is due to the asymmetry at Eu.**S1** in the complexes, and not due to quenching from the lattice.

Further support for the link between asymmetry and lowering of the luminescence lifetime is found in the literature. Zucchi *et al.* have studied luminescence properties of Eu(III) in DOTAM-derivatives with *p*-nitrophenyl pendant arms. In **Eu.L** (L = 2,2',2",2"'-(1,4,7,10-tetraazacyclododecane-1,4,7,10-tetrayl)tetrakis(N-(4-nitrophenyl)acetamide) Eu(III) is coordinated by four nitrogen atoms and five oxygen atoms (one capping methoxide).[67] The Eu-N and Eu-O bond lengths in **Eu.L** are close to **1-H,** but the capping oxygen bond of 2.451 Å is slightly shorter in **Eu.L** than the average 2.535 Å in **1-H**. This structure also has the metal ion in a cTSAP environment with a N- and O-donor atom plane twist angle of 25.5º, however, here the geometry is enforced by the bulky pedant arms, and not the crystal packing. Thus, **Eu.L** maintains the cTSAP structure in both solid state and solution.[67]

Luminescence lifetimes of **Eu.L** were measured on dried crystals at 293 K and 77 K, and in D_2O. The lifetime of dry **Eu.L** crystals at 293 K of 450 μS (ex. = 385 nm) is close to the 460.3 μS for the **1-H** single crystal. At 77 K the lifetime of **Eu.L** is 490 μS (ex. = 385 nm) is slightly shorter than for **1-H** powder, also at 77K, of 558.5 μS. The largest difference is seen between the deuterated samples. **Eu.L** in D_2O has a lifetime of 769 μS (ex. = 375 nm), whereas the average of the lifetime for **1-D** measured at position 1 and 2 is 921.5 μS. If we disregard, the possibility of additional quenching from the ligands, there are significant differences in the extended ligand systems between the two compounds, but the immediate environments around Eu(III) are very similar.

To compare the effect of coordination geometry on luminescence lifetime, first other quenching effects must be removed. As we are comparing DOTA to DOTA-amides, the main difference is the presence or absence of N-H oscillators.[55] Further, the distance to the cap-

ping water may influence the observed lifetime.[68] As all these effects are expected to vanish in deuterated media, we compare the lifetimes in D_2O, see Table 4. Note that **1-D** is a solid, while the other complexes are in solution.

Table 4. Luminescence lifetimes of Eu(III) in 4N-4O-1O coordination geometries (CN = 9) in deuterated media at 293 K.

Complex	Structure	τ_{lm} (μS)
$[Eu(DOTA)(D_2O)]^-$ in **1-D**	cTSAP	962
$[\mathbf{Eu.L}(D_2O)]^{3+}$	cTSAP	769
$[Eu(DOTA)(D_2O)]^-$	cSAP	2,174
$[Eu(DOTAM)(D_2O)]^{3+}$	cTSAP	2,439

In solution, we expect that fluctuations in the coordination sphere result in complexes with an on-average high coordination symmetry. In the solid state, there are no degrees of freedom or fluctuations, and the coordination geometry is locked. As we do not see any other obvious quenching pathways in **1-D** compared to $[Eu(DOTA)(D_2O)]^-$ in solution, we suggest that the effect from the donor-atom geometry significantly affects the rate of spontaneous emission of europium(III) centers. The data presented here indicate that symmetry – or lack thereof – strongly affects the observed luminescence lifetime and is comparable to the effect of introducing quenching agents. Also, at Eu.**S1**, $q = 1$ was determined, which strongly support a low water content in the complex and makes other energy migration pathways improbable. We also observe two distinct lifetimes, which prohibits energy migration between europium(III) centers. Thus, we arrive at the conclusion that the luminescence rate constant k_{Lm} (or Einstein's probability of spontaneous emission - A) for $[Eu(DOTA)(H_2O)]^-$ in the asymmetric Eu.**S1** is twice that of $[Eu(DOTA)(H_2O)]^-$ in solution. The difference in the powder spectrum of **1-H** and the single crystal spectra of **1-H** and **1-D** is clearly seen in Figure 4. Because of the three coordinating water molecules in **Eu.S2**, we expect a larger degree of quenching of luminescence than for **Eu.S1** at room temperature. At lower temperatures, the quenching is reduced and the contribution to spectral profile coming from **Eu.S2** becomes more pronounced. It is also worth adding that the powder spectrum represents the average structure, whereas the single crystals represent the structure at that given orientation of the crystal. Note the twinning of the crystal implies that more than one molecular orientation is always present. The most pronounced effects of crystal orientation (from Figure 5) was observed for the $\Delta J = 4$ transitions, where there is very noticeable increase in the 704 nm peak upon rotation. We assign this emission line to Eu.**S2**, as Bettinelli *et al.* observed a very intense peak for the transition at 704 nm to an eight-coordinated Eu(III) in a distorted square antiprismatic geometry.[69] Here, the metal ion is doped into a $Ca_3Sc_2Si_3O_{12}$ garnet structure, and is solely coordinated by oxygen atoms. The unusual intensity is attributed to the reduced symmetry in the geometry of the donor-atom environment. Figure 5 shows that we observe a similar increase in peak intensity at 704 nm for **1-D** at position 2. To investigate this further, the deuterated crystal was rotated 90 degrees in increments of 10 degrees. At every step an emission spectrum was recorded to observe changes in

the peak profile. The full spectra and an enlarged view of the 700 nm band are shown in Figure 6.

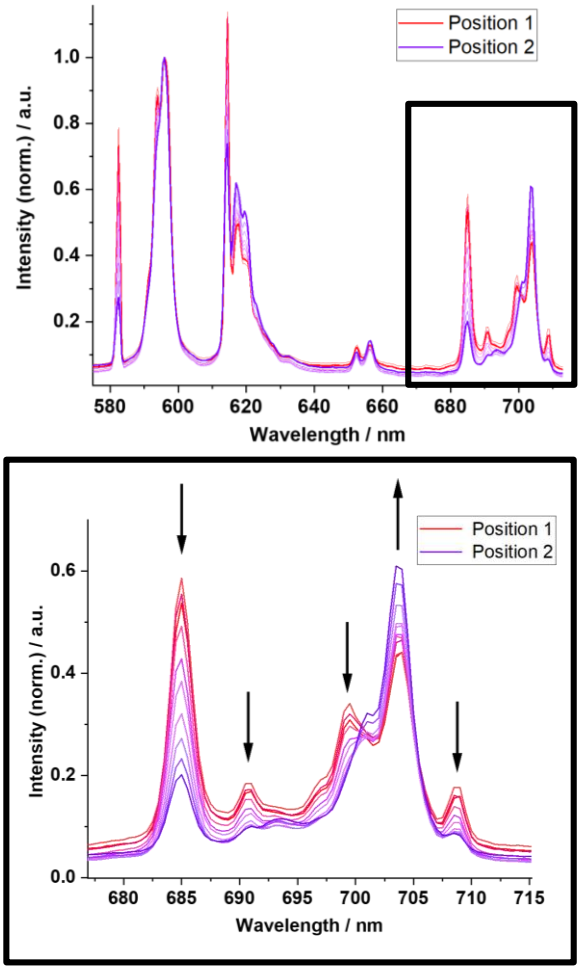

Figure 6. Top: Normalized emission spectra of **1-D** turned 90 degrees with respect to the beam in increments of 10 degrees from position 1 (red) to position 2 (purple). Excitation = 394 nm **Bottom:** Enlarged spectrum from 680 nm to 715 nm.

The starting point corresponds to the spectrum recorded at position 1 (Figure 5). Here, Eu**.S1** is the dominant site as only one lifetime can be observed. As the crystal is rotated, the peak profile starts to resemble the powder spectrum. Based on this and the observations from Bettinelli *et al*, we can see that the **Eu.S2** component increases as the crystal is rotated. Thus, we can relate the observed luminescence to the contribution coming from each Eu(III) site and directly see that the amount of intensity coming from Eu.**S1** and Eu.**S2** changes depending on the angle of the crystal towards the incident beam.

CONCLUSION

We have developed a procedure that reproducibly provides crystals of a homometallic heterotrinuclear europium(III) complex. The structure of $[Eu(\mu O)_5(OH_2)_3][Eu(DOTA)(H_2O)]_2Cl$ is the first reported, which contains a capped twisted square antiprism (cTSAP) form of $[Eu(DOTA)(H_2O)]^-$ with Eu(III) centers acting as cation and anion. Having prepared crystals of the protonated and deuterated forms of the complex, the luminescence emission spectra and lifetimes of each of the two sites – free Eu(III) ions and $[Eu(DOTA)(H_2O)]^-$ complexes – in the crystal was determined. We found that crystal packing can largely effect the geometry of the DOTA ligand system, and that the enforced asymmetric coordination environment in $[Eu(\mu O)_5(OH_2)_3][Eu(DOTA)(H_2O)]_2Cl$ results in decreased luminescence lifetimes. A fact that we tentatively ascribe to an asymmetry induced increase in the rate constant of luminescence. The presence of two luminescent sites in the complex $[Eu(\mu O)_5(OH_2)_3][Eu(DOTA)(H_2O)]_2Cl$ complicates further analysis. Therefore, the next step is to prepare $[Ln(\mu O)_5(OH_2)_3][Ln'(DOTA)(H_2O)]_2Cl$ to further elucidate the effect of asymmetry in lanthanide luminescence.

Supporting Information.

The following files are available free of charge: Compilation of emission spectra, emission decay profiles, description of single crystal spectroscopy setup, crystal packing, powder XRD diffractogram, chart of structure of macrocyclic ligands, and absorption spectrum (PDF) and crystal structure (CIF).

Corresponding Author

*Thomas Just Sørensen, tjs@chem.ku.dk, @f_elements, Nano-Science Center and Department of Chemistry, University of Copenhagen, Universitetsparken 5, 2100 København Ø, Denmark.

Funding Sources

We thank Carlsbergfondet, Villum Fonden (grant#14922), and the University of Copenhagen for funding.

ACKNOWLEDGMENT

We thank Carlsbergfondet, Villum Fonden (grant#14922), and the University of Copenhagen for support. We thank Helene O.B. Andersen for help during the preparation of the manuscript.

REFERENCES

1. Pagis, C.; Ferbinteanu, M.; Rothenberg, G.; Tanase, S., Lanthanide-Based Metal Organic Frameworks: Synthetic Strategies and Catalytic Applications. *ACS Catalysis* **2016,** *6* (9), 6063-6072.

2. Mikami, K.; Terada, M.; Matsuzawa, H., "Asymmetric" Catalysis by Lanthanide Complexes. *Angewandte Chemie International Edition* **2002,** *41* (19), 3554-3572.

3. Gupta, C. K.; Krishnamurthy, N., Extractive metallurgy of rare earths. *International Materials Reviews* **1992,** *37* (1), 197-248.

4. Molander, G. A., Application of lanthanide reagents in organic synthesis. *Chemical Reviews* **1992,** *92* (1), 29-68.

5. Dai, L.; Jones, C. M.; Chan, W. T. K.; Pham, T. A.; Ling, X.; Gale, E. M.; Rotile, N. J.; Tai, W. C.-S.; Anderson, C. J.; Caravan, P.; Law, G.-L., Chiral DOTA chelators as an improved platform for biomedical imaging and therapy applications. *Nature Communications* **2018,** *9* (1), 857.

6. Caravan, P.; Ellison, J. J.; McMurry, T. J.; Lauffer, R. B., Gadolinium(III) Chelates as MRI Contrast Agents: Structure, Dynamics, and Applications. *Chemical Reviews* **1999,** *99* (9), 2293-2352.

7. Nassar, N. T.; Brainard, J.; Gulley, A.; Manley, R.; Matos, G.; Lederer, G.; Bird, L. R.; Pineault, D.; Alonso, E.; Gambogi, J.; Fortier, S. M., Evaluating the mineral commodity supply risk of the U.S. manufacturing sector. *Science Advances* **2020,** *6* (8), eaay8647.

8. Frohlich, P.; Lorenz, T.; Martin, G.; Brett, B.; Bertau, M., Valuable Metals-Recovery Processes, Current Trends, and Recycling Strategies. *Angewandte Chemie* **2017,** *56* (10), 2544-2580.

9. Cheisson, T.; Schelter, E. J., Rare earth elements: Mendeleev's bane, modern marvels. *Science* **2019,** *363* (6426), 489-493.

10. Bünzli, J.-C. G., Lanthanide coordination chemistry: From old concepts to coordination polymers. *Journal of Coordination Chemistry* **2014**, 1-45.

11. Helm, L.; Merbach, A. E., Inorganic and bioinorganic solvent exchange mechanisms. *Chem Rev* **2005,** *105* (6), 1923-59.

12. Meier, D. J.; Garner, C. S., The Kinetics of the Europium (II)-Europium (III) Exchange Reaction. *The Journal of Physical Chemistry* **1952,** *56* (7), 853-857.

13. Caravan, P.; Ellison, J. J.; McMurry, T. J.; Lauffer, R. B., Gadolinium(III) chelates as

MRI contrast agents: Structure, dynamics, and applications. *Chemical Reviews* **1999,** *99* (9), 2293-2352.

14. Sørensen, T. J.; Faulkner, S., Multimetallic Lanthanide Complexes: Using Kinetic Control To Define Complex Multimetallic Arrays. *Acc Chem Res* **2018,** *51* (10), 2493-2501.

15. Nielsen, L. G.; Sørensen, T. J., Including and Declaring Structural Fluctuations in the Study of Lanthanide(III) Coordination Chemistry in Solution. *Inorganic chemistry* **2019,** *59* (1), 94-105.

16. Nawrocki, P. R.; Kofod, N.; Juelsholt, M.; Jensen, K. M. Ø.; Sørensen, T. J., The effect of weighted averages when determining the speciation and structure–property relationships of europium(iii) dipicolinate complexes. *Physical Chemistry Chemical Physics* **2020,** *22* (22), 12794-12805.

17. Garda, Z.; Nagy, V.; Rodríguez-Rodríguez, A.; Pujales-Paradela, R.; Patinec, V.; Angelovski, G.; Tóth, É.; Kálmán, F. K.; Esteban-Gómez, D.; Tripier, R.; Platas-Iglesias, C.; Tircsó, G., Unexpected Trends in the Stability and Dissociation Kinetics of Lanthanide(III) Complexes with Cyclen-Based Ligands across the Lanthanide Series. *Inorganic chemistry* **2020,** *59* (12), 8184-8195.

18. Cotton, S., *Lanthanide and Actinide Chemistry*. Wiley: Chichester, 2006.

19. Bordes, A.; Poveda, A.; Troadec, T.; Franconetti, A.; Arda, A.; Perrin, F.; Menand, M.; Sollogoub, M.; Guillard, J.; Desire, J.; Tripier, R.; Jimenez-Barbero, J.; Bleriot, Y., Synthesis, Conformational Analysis, and Complexation Study of an Iminosugar-Aza-Crown, a Sweet Chiral Cyclam Analog. *Organic letters* **2020**.

20. Franklin, S. J.; Raymond, K. N., Solution Structure and Dynamics of Lanthanide Complexes of the Macrocyclic Polyamino Carboxylate DTPA-dien. NMR

Study and Crystal Structures of the Lanthanum(II1) and Europium(II1) Complexes. *Inorganic chemistry* **1994,** *33*, 5794-5804.

21. Webber, B. C.; Payne, K. M.; Rust, L. N.; Cassino, C.; Carniato, F.; McCormick, T.; Botta, M.; Woods, M., Analysis of the Relaxometric Properties of Extremely Rapidly Exchanging Gd3+ Chelates: Lessons from a Comparison of Four Isomeric Chelates. *Inorganic chemistry* **2020,** *59* (13), 9037-9046.

22. Nielsen, L. G.; Junker, A. K. R.; Sørensen, T. J., Composed in the f-block: solution structure and function of kinetically inert lanthanide(iii) complexes. *Dalton transactions* **2018,** *47* (31), 10360-10376.

23. Kofod, N.; Nawrocki, P.; Juelsholt, M.; Christiansen, T. L.; Jensen, K. M. Ø.; Sørensen, T. J., Solution Structure, Electronic Energy Levels, and Photophysical Properties of [Eu(MeOH)n−2m(NO3)m]3–m+ Complexes. *Inorganic chemistry* **2020,** *59* (15), 10409-10421.

24. Junker, A. K. R.; Hill, L. R.; Thompson, A. L.; Faulkner, S.; Sørensen, T. J., Shining light on the antenna chromophore in lanthanide based dyes. *Dalton transactions* **2018,** *47* (14), 4794-4803.

25. Stetter, H.; Frank, W., Complex Formation with Tetraazacycloalkane-N,N′,N″,N‴-tetraacetic Acids as a Function of Ring Size. *Angewandte Chemie International Edition in English* **1976,** *15* (11), 686-686.

26. Cotton, F. A.; Wilkinson, G., *Advanced Inorganic Chemistry*. 4th ed.; 1980.

27. de Bettencourt-Dias, A., *Luminescence of Lanthanide Ions in Coordination Compounds and Nanomaterials* John Wiley and Sons, Ltd. : 2014.

28. Corner, W. D.; Tanner, B. K., *Rare Earths and Actinides*. 1977.

29. Carnall, W. T., A systematic analysis of the spectra of trivalent actinide chlorides in D3h site symmetry. *The Journal of Chemical Physics* **1992,** *96* (12), 8713-8726.

30. Carnall, W. T.; Goodman, G. L.; Rajnak, K.; Rana, R. S., A systematic analysis of the spectra of the lanthanides doped into single crystal LaF3 *The Journal of chemical physics* **1989,** *90* (7), 3443-3457.

31. Binnemans, K., Interpretation of europium(III) spectra. *Coordination Chemistry Reviews* **2015,** *295*, 1-45.

32. Vicentini, G.; Zinner, L. B.; Zukerman-Schpector, J.; Zinner, K., Luminescence and structure of europium compounds. *Coordination Chemistry Reviews* **2000,** *196* (1), 353-382.

33. Martins, J. P.; Martín-Ramos, P.; Chamorro-Posada, P.; Pereira Silva, P. S.; Martín-Gil, J.; Hernández-Navarro, S.; Ramos Silva, M., Experimental and Theoretical Studies on the Structure and Photoluminescent Properties of New Mononuclear and Homodinuclear Europium(III) β-Diketonate Complexes. *Advances in Condensed Matter Physics* **2015,** *2015*, 205047.

34. Sheng, K. C.; Korenowski, G. M., Laser-induced optical emission studies of europium(3+) sites in polycrystalline powders of monoclinic and bcc. europium sesquioxide. *The Journal of Physical Chemistry* **1988,** *92* (1), 50-56.

35. Sudnick, D. R., Time-Resolved Europium(III) Excitation Spectroscopy: A Luminescence Probe of Metal Ion Binding Sites. *Science* **1979,** *206* (4423), 1194-1196.

36. Petiote, L.; Cabral, F. M.; Formiga, A. L. B.; Mazali, I. O.; Sigoli, F. A., A series of three isostructural 1D lanthanide coordination network based on 4,4′,4″-((benzene-1,3,5-triyltris(methylene))tris(oxy))tribenzoate ligand: Synthesis, crystal structure and

photophysical properties. *Inorganica Chimica Acta* **2019,** *494*, 21-29.

37. Monteiro, J. H. S. K.; Dutra, J. D. L.; Freire, R. O.; Formiga, A. L. B.; Mazali, I. O.; de Bettencourt-Dias, A.; Sigoli, F. A., Estimating the Individual Spectroscopic Properties of Three Unique EuIII Sites in a Coordination Polymer. *Inorganic Chemistry* **2018,** *57* (24), 15421-15429.

38. Wahsner, J.; Gale, E. M.; Rodríguez-Rodríguez, A.; Caravan, P., Chemistry of MRI Contrast Agents: Current Challenges and New Frontiers. *Chemical Reviews* **2019,** *119* (2), 957-1057.

39. Huang, S.; Chen, H. H.; Yuan, H.; Dai, G.; Schuhle, D. T.; Mekkaoui, C.; Ngoy, S.; Liao, R.; Caravan, P.; Josephson, L.; Sosnovik, D. E., Molecular MRI of acute necrosis with a novel DNA-binding gadolinium chelate: kinetics of cell death and clearance in infarcted myocardium. *Circulation. Cardiovascular imaging* **2011,** *4* (6), 729-37.

40. Heffern, M. C.; Matosziuk, L. M.; Meade, T. J., Lanthanide probes for bioresponsive imaging. *Chem Rev* **2014,** *114* (8), 4496-539.

41. DREW, M. G. B., STRUCTURES OF HIGH COORDINATION COMPLEXES. *Coordination Chemistry Reviews* **1977,** *24* 179-275.

42. Aime, S.; Botta, M.; Ermondi, G., NMR Study of Solution Structures and Dynamics of Lantbanide(III) Complexes of DOTA. *Inorg. Chem* **1992,** *31*, 4291-4299.

43. Dai, L.; Zhang, J.; Chen, Y.; Mackenzie, L. E.; Pal, R.; Law, G.-L., Synthesis of Water-Soluble Chiral DOTA Lanthanide Complexes with Predominantly Twisted Square Antiprism Isomers and Circularly Polarized Luminescence. *Inorganic Chemistry* **2019,** *58* (19), 12506-12510.

44. Benetollo, F.; Bombieri, G.; Calabi, L.; Aime, S.; Botta, M., Structural Variations Across the Lanthanide Series of Macrocyclic DOTA Complexes: Insights into the Design of Contrast Agents for Magnetic Resonance Imaging. *Inorganic Chemistry* **2003,** *42* (1), 148-157.

45. Bruker *SAINT, Version 7.68A*, Bruker, Madison, Wisconsin, USA, 2009.

46. Sheldrick, G. M. *CELL_NOW*, Georg-August-Universität, Göttingen, Germany., 2008.

47. Sheldrick, G. M. *TWINABS*, Bruker, Madison, Wisconsin, USA, 2012.

48. Dolomanov, O. V.; Bourhis, L. J.; Gildea, R. J.; Howard, J. A. K.; Puschmann, H., Olex2. *J. Appl. Crystallogr.* **2009,** *42*, 339-341.

49. Sheldrick, G. M., A short history of SHELX. *Acta Cryst. A* **2008,** *A64*, 112-122.

50. Sheldrick, G. M., SHELXL. *Acta Cryst.* **2015,** *C71*, 3-8.

51. Corporation, O. *Origin*, OriginLab Corporation, Northampton, MA, USA., 2017.

52. Giacovazzo, C., *Fundamentals of Crystallography*. Oxford University Press: 2002.

53. Sevvana, M.; Ruf, M.; Usón, I.; Sheldrick, G. M.; Herbst-Irmer, R., Non-merohedral twinning: from minerals to proteins. *Acta Cryst.* **2019,** *D75*, 1040-1050.

54. Horrocks, W. D.; Sudnick, D. R., Lanthanide ion probes of structure in biology. Laser-induced luminescence decay constants provide a direct measure of the number of metal-coordinated water molecules. *Journal of the American Chemical Society* **1979,** *101* (2), 334-340.

55. Beeby, A.; Clarkson, I. M.; Dickins, R. S.; Faulkner, S.; Parker, D.; Royle, L.; de Sousa, A. S.; Williams, J. A. G.; Woods, M., Non-radiative deactivation of the excited

states of europium, terbium and ytterbium complexes by proximate energy-matched OH, NH and CH oscillators: an improved luminescence method for establishing solution hydration states. *Journal of the Chemical Society, Perkin Transactions 2* **1999,** (3), 493-504.

56. Tropiano, M.; Blackburn, O. A.; Tilney, J. A.; Hill, L. R.; Just Sørensen, T.; Faulkner, S., Exploring the effect of remote substituents and solution structure on the luminescence of three lanthanide complexes. *J. Luminescence* **2015,** *167*, 296-304.

57. Moulin, C.; Wei, J.; Iseghem, P. V.; Laszak, I.; Plancque, G.; Moulin, V., Europium complexes investigations in natural waters by time-resolved laser-induced fluorescence. *Analytica Chimica Acta* **1999,** *396* (2), 253-261.

58. Kropp, J. L.; Windsor, M. W., Luminescence and Energy Transfer in Solutions of Rare-Earth Complexes. I. Enhancement of Fluorescence by Deuterium Substitution. *The Journal of Chemical Physics* **1965,** *42* (5), 1599-1608.

59. Albin, M.; Horrocks, W. D.; Liotta, F. J., Characterization of a potentially axially symmetric europium(III) complex of a tetraacetate,tetraaza, macrocyclic ligand by luminescence excitation, emission and lifetime spectroscopy. *Chemical Physics Letters* **1982,** *85* (1), 61-64.

60. Supkowski, R. M.; Horrocks, W. D., On the determination of the number of water molecules, q, coordinated to europium(III) ions in solution from luminescence decay lifetimes. *Inorganica Chimica Acta* **2002,** *340*, 44-48.

61. Amin, S.; Voss, D. A.; Horrocks, W. D.; Lake, C. H.; Churchill, M. R.; Morrow, J. R., Laser-Induced Luminescence Studies and Crystal Structure of the Europium(III) Complex of 1,4,7,10-Tetrakis(carbamoylmethyl)-1,4,7,10-

tetraazacyclododecane. The Link between Phosphate Diester Binding and Catalysis by Lanthanide(III) Macrocyclic Complexes. *Inorganic Chemistry* **1995,** *34* (12), 3294-3300.

62. Woods, M.; Aime, S.; Botta, M.; Howard, J. A. K.; Moloney, J. M.; Navet, M.; Parker, D.; Port, M.; Rousseaux, O., Correlation of Water Exchange Rate with Isomeric Composition in Diastereoisomeric Gadolinium Complexes of Tetra(carboxyethyl)dota and Related Macrocyclic Ligands. *Journal of the American Chemical Society* **2000,** *122* (40), 9781-9792.

63. Thuéry, P., Structural variability in uranyl–lanthanide heterometallic complexes with DOTA and oxalato ligands. *CrystEngComm* **2009,** *11* (11), 2319-2325.

64. Woods, M.; Payne, K. M.; Valente, E. J.; Kucera, B. E.; Young Jr., V. G., Crystal Structures of DOTMA Chelates from Ce3+ to Yb3+: Evidence for a Continuum of Metal Ion Hydration States. *Chemistry – A European Journal* **2019,** *25* (42), 9997-10005.

65. Aime, S.; Barge, A.; Benetollo, F.; Bombieri, G.; Botta, M.; Uggeri, F., A Novel Compound in the Lanthanide(III) DOTA Series. X-ray Crystal and Molecular Structure of the Complex Na[La(DOTA)La(HDOTA)]·10H2O. *Inorganic Chemistry* **1997,** *36* (19), 4287-4289.

66. Shannon, R. D., Revised effective ionic radii and systematic studies of interatomic distances in halides and chalcogenides. *Acta Crystallographica Section A* **1976,** *A32*, 751-767.

67. Zucchi, G.; Scopelliti, R.; Bünzli, J.-C. G., Importance of the chromophore orientation to the ligand-to-metal energy transfer in lanthanide complexes with pendant-arm fitted cyclen derivatives *Journal of the Chemical Society, Dalton Transactions* **2001,** (13), 1975-1985.

68. Parker, D., Excitement in f block: structure, dynamics and function of nine-coordinate chiral lanthanide complexes in aqueous media. *Chemical Society reviews* **2004,** *33* (3), 156-65.

69. Bettinelli, M.; Speghini, A.; Piccinelli, F.; Neto, A. N. C.; Malta, O. L., Luminescence spectroscopy of Eu3+ in Ca3Sc2Si3O12. *Journal of Luminescence* **2011,** *131* (5), 1026-1028.

TOC SYNOPSIS

Structure-property relationships in Ln(DOTA) complexes remain elusive. In this paper, we report the crystal structure and optical properties of $[Eu(DOTA)(H_2O)]^-$ in the capped twisted square antiprismatic form. The structure was isolated in a $[Eu(\mu O)_5(OH_2)_3][Eu(DOTA)(H_2O)]_2Cl$ complex, which was prepared in both protonated and deuterated forms to separate the optical properties of the two different europium(III) sites found in the structure.

TOC